

Ionospheric Sluggishness: A Characteristic Time-Lag of the Ionospheric Response to Solar Flares

Shibaji Chakraborty¹, John Michael Ruohoniemi¹, Joseph Baker¹, Scott Bailey², Robyn Fiori³, and Kate Zawdie⁴

¹Virginia Tech

²Virginia Polytechnic Institute and State University

³Natural Resources Canada

⁴US Naval Research Laboratory

November 22, 2022

Abstract

The term “ionospheric sluggishness” is used to describe the time delay between maximum radio absorption in the ionosphere following the time of maximum irradiance during a solar flare. Sluggishness is one of the characteristic properties known to be maximized around D-region heights and can be used for studying lower ionospheric (D-region) and mesospheric chemistry. This article is our first attempt to estimate ionospheric sluggishness using high frequency (HF, 3 – 30 MHz) instruments. Specifically, we report on first estimates of sluggishness from riometer and SuperDARN observations following a solar flare and propose two new methods to estimate sluggishness. Sluggishness is shown to be anti-correlated with the peak solar X-ray flux and positively correlated with solar zenith angle and geographic latitude. The choice of instrument, method, and reference solar waveband effects the sluggishness estimation. A simulation study was performed to estimate the effective recombination coefficient, which was found to vary between 4-5 orders of magnitude. We suggest that the effective recombination coefficient is highly sensitive to D-region’s negative and positive ion chemistry.

Ionospheric Sluggishness: A Characteristic Time-Lag of the Ionospheric Response to Solar Flares

S. Chakraborty^{*1}, J. M. Ruohoniemi¹, J. B. H. Baker¹, S. M. Bailey¹, R. A. D. Fiori², and K. A. Zawdie³

¹Bradley Department of Electrical and Computer Engineering, Virginia Tech, Blacksburg, Virginia, USA

²Geomagnetic Laboratory, Natural Resources Canada, Ottawa, Ontario, Canada

³Space Science Division, US Naval Research Laboratory, Washington DC, USA

Corresponding author: Shibaji Chakraborty (shibaji7@vt.edu)

Key Points:

- The choice of ionospheric sounding techniques and reference solar irradiance wavebands affects the estimation of ionospheric sluggishness
- A simulation study shows that the D-region effective recombination coefficient varies by 4 – 5 orders of magnitude
- It is suggested that ionospheric sluggishness might be influenced by the ionic (negative and positive cluster ions) photochemistry

Abstract

The term “ionospheric sluggishness” is used to describe the time delay between maximum radio absorption in the ionosphere following the time of maximum irradiance during a solar flare. Sluggishness is one of the characteristic properties known to be maximized around D-region heights and can be used for studying lower ionospheric (D-region) and mesospheric chemistry. This article is our first attempt to estimate ionospheric sluggishness using high frequency (HF, 3 – 30 MHz) instruments. Specifically, we report on first estimates of sluggishness from riometer and SuperDARN observations following a solar flare and propose two new methods to estimate sluggishness. Sluggishness is shown to be anti-correlated with the peak solar X-ray flux and positively correlated with solar zenith angle and geographic latitude. The choice of instrument, method, and reference solar waveband effects the sluggishness estimation. A simulation study was performed to estimate the effective recombination coefficient, which was found to vary between 4 – 5 orders of magnitude. We suggest that the effective recombination coefficient is highly sensitive to D-region’s negative and positive ion chemistry.

Plain Language Summary

A systematic time delay between peak incoming solar radiation during a solar flare and peak electron density in the ionosphere is known as ionospheric sluggishness. Ionospheric sluggishness is known to be maximized around D-region heights (~60-90 km altitude). This article is our first attempt to estimate ionospheric sluggishness using high frequency (3 – 30 MHz) instruments. In addition, we statistically characterize the observed sluggishness and provide an insight into D-region photochemical processes. In this article, we also demonstrate how to extract D-region’s recombination coefficient using a theoretical model and measured sluggishness.

1. Introduction

Solar EUV and X-rays radiations are primary sources for producing the ionosphere. The characteristic ionospheric response to a sudden intense solar X-ray burst, or solar flare, has been studied since the early 1900s (Dellinger, 1937). Flare-driven high frequency (HF; 3-30 MHz) absorption, also known as shortwave-fadeout (SWF), is a well-understood phenomenon (e.g., Mitra, 1974; Fiori et al., 2018). However, the initial time delay of the ionospheric response following a solar flare, also known as “sluggishness”, is not yet fully understood (Palit et al., 2015). E. V. Appleton first defined the term sluggishness as the time delay between the peak ionospheric electron density and peak electron-ion production rate at local solar noon (Appleton, 1953). We now understand sluggishness as an inertial property of the ionosphere that is dependent on latitude, longitude, and height of the ionosphere, as described in equation (1) (Appleton, 1953).

$$\delta = \delta(\theta, \phi, h) = T_{n_e^{max}} - T_{q^{max}} \quad (1)$$

where: $\theta, \phi, h, T_{n_e^{max}}$, and $T_{q^{max}}$ are latitude, longitude, altitude, times of peak electron density, and peak electron-ion production rate, respectively. In addition, Appleton found that δ is inversely proportional to electron density and the effective recombination coefficient (α_{eff}). Appleton and his contemporaries tried to measure and characterize sluggishness in terms of the time delay between peak radio wave absorption (β) in the ionosphere and peak solar irradiance (I_{∞}^{max}) (Appleton, 1953; Ellison, 1953), as described in equation (2).

$$\bar{\delta} = \bar{\delta}(\theta, \phi) = T_{\beta^{max}} - T_{I_{\infty}^{max}} \quad (2)$$

where: $T_{\beta^{max}}$ and $T_{I_{\infty}^{max}}$ are the times of peak HF absorption and peak solar irradiance, respectively.

Consequently, ionospheric sluggishness is the time difference between the peak of solar flux and ionospheric response. However, recent studies have shown that some HF instruments undergo a saturation effect (a flat peak in the observation, see section 3.1 for details) due to substantial ionospheric HF absorption effect, in response to an X-class solar flare (Chakraborty et al., 2018, 2019). Hence, the standard definition by equation (2) will not provide an accurate measurement of sluggishness using SuperDARN data. Hence, we propose two alternative definitions of sluggishness. First, we define it as the time difference between the peak in the time derivative of β and the peak in the time derivative of I_{∞} (i.e. $\bar{\delta}_s$ a name), as described in equation (3).

$$\bar{\delta}_s = \bar{\delta}_s(\theta, \phi) = T_{\dot{\beta}} - T_{\dot{I}_{\infty}} \quad (3)$$

where: $T_{\dot{\beta}}$ and $T_{\dot{I}_{\infty}}$ are the times of peak time derivative in absorption and peak time derivative in solar irradiance, respectively. Second, we define the time shift (τ) in I_{∞} that maximizes the correlation (ρ) between β and I_{∞} , as described in equation (4).

$$\bar{\delta}_c = \bar{\delta}_c(\theta, \phi) = \max_{\tau} \rho[\beta(t), I_{\infty}(t + \tau)] \quad (4)$$

Note that $\bar{\delta}$, $\bar{\delta}_s$, and $\bar{\delta}_c$ represent time delays between a change in solar irradiance and an ionospheric response, whereas δ represents the time delay between peak photoionization rate and peak ionospheric electron density. Specifically, $\bar{\delta}$ represents the time delay between the peak in the HF absorption and peak solar irradiance of the event, whereas $\bar{\delta}_s$ represents the time delay when both solar irradiance and ionospheric response are changing most rapidly (during the peak of time derivative) and $\bar{\delta}_c$ represents the time delay that maximizes statistical similarities between solar irradiance and ionospheric response. Although the three different time delays defined in equations (2)-(4) have different reference times, measurement, and estimation techniques, all of them are indicative of the inertial property of the ionosphere. Finally, our proposed definitions in terms of peak time derivative and correlation are advantageous for characterizing the response of the ionosphere to impulsive events such as flares measured using instruments such as riometers and SuperDARN HF radars.

Figure 1(a-c) present examples of the estimation of height integrated ionospheric sluggishness $\bar{\delta}$, $\bar{\delta}_s$, and $\bar{\delta}_c$ using the conventional, peak time derivative, and correlation methods, respectively. The data were obtained with the Ottawa riometer data during a solar flare event on 11 March 2015. The red curve and black dots in all three panels indicate solar soft X-ray (.1-.8 nm) irradiance from a GOES satellite and cosmic noise absorption (CNA) from the Ottawa riometer, respectively. The solid and dashed vertical lines in panel (a) and (b) indicate peaks and maximum time derivative in X-ray irradiance (red) and CNA data (black), respectively. The difference in the solid [dashed] vertical lines in panel (a) [(b)] represents the estimated conventional [time derivative] sluggishness. Furthermore, the red dashed curve in panel (c) shows the time-shifted solar soft X-ray (.1-.8 nm) irradiance. The correlation coefficient and estimated sluggishness are shown in the panel. The estimated sluggishness from the three different methods are $\bar{\delta} = 46s$, $\bar{\delta}_s = 139s$, and $\bar{\delta}_c = 80s$, for this event, respectively.

Since Appleton first described sluggishness, experimental studies have used very low frequency (VLF, 3-30 kHz) receivers to understand its variations with solar zenith angle (χ), and peak solar irradiance I_{∞}^{max} (Ellison, 1953; Palit et al., 2015). The sluggishness recorded using VLF instruments is defined as the time difference between the peak in VLF amplitude (A^{max}) and I_{∞}^{max} , as described in equation (5).

$$\delta^{VLF} = T_{A^{max}} - T_{I_{\infty}^{max}} \quad (5)$$

VLF Studies have reported a typical value of sluggishness (δ^{VLF}) is 3-10 minutes (Basak & Chakrabarti, 2013; Palit et al., 2015). Most of these studies reported wide variability of sluggishness values during M and C class flares but did not try to explain the chemical processes that manifest the sluggishness.

Sluggishness measurements are useful because they provide information about the ionospheric electron density and the effective recombination coefficient (α_{eff}) (Appleton, 1953); the latter being controlled by the atmospheric negative ions (e.g. O^- , O_2^- , NO_3^- , CO_3^- , HNO_3^- etc and their hydrates) and positive ions (e.g. $H^+(H_2O)_n$) (Palit et al., 2015; Reid, 1970; Verronen et al., 2006). Specifically, α_{eff} defines the effective loss rate of electrons due to cascading photochemical reactions following electron production due to photoionization (Pequignot et al., 1991). Sluggishness measurements can thus provide insight into D-region and mesospheric photochemistry and be used to validate models.

Here we report on the first study to compare the basic characteristic of sluggishness using both passive and active high frequency (HF, 3-30 MHz) instruments,

namely, riometers and SuperDARN HF radars, respectively. We present a statistical characterization of ionospheric sluggishness following C, M, and X class flares and report on the variations of conventional sluggishness (δ) with χ , I_{∞}^{max} , local time (LT) and latitude (ϕ). Through a theoretical modeling study and measured $\bar{\delta}$ from riometer data, we show how α_{eff} varies with peak solar soft X-ray flux. Finally, we discuss how our results inform the physics of sluggishness and its variability, and our understanding of D-region photochemical processes.

2. Instrumentations

In this study, we used GOES-15 X-ray sensor data for the solar X-ray irradiance information during solar flares and ionospheric absorption in the HF bands from ground-based riometers and SuperDARN HF radars, respectively (Bland et al., 2018). Solar X-ray flux information was obtained from the solar X-ray sensor of the National Oceanic and Atmospheric Administration's (NOAA) GOES 15 satellite (Machol, 2016). This instrument has two channels, namely hard (0.05-0.4 nm) and soft (.1-.8 nm), to detect variations in solar flux in these two wavebands. We primarily used soft X-ray (SXR) flux for our analysis; however, hard X-ray (HXR) information is also used for comparison.

A riometer is a ground-based passive radio receiver, which provides information about the ionospheric HF absorption by measuring variations in cosmic radio noise at 30 MHz frequency (e.g., Browne et al., 1995; Fiori & Danskin, 2016). The CNA values used in this study are taken from a network of riometers distributed across Canada operated partially by Natural Resources Canada (NRCan) and partially by the University of Calgary (Geospace Observatory riometer, or GO-RIO) (Danskin, 2008; Lam, 2011; Rostoker et al., 1995).

SuperDARN is a global network of HF radars, operating between 8 and 18 MHz, located across the middle, high and polar latitudes of both hemispheres. Each radar observes the line-of-sight (LoS) component of plasma velocity along 16 to 20 beams in 75-110 range gates spaced 45 km apart beginning at 180 km range (Chisham et al., 2007; Greenwald et al., 1985; Nishitani et al., 2019). Typically, each beam sounding has a 3s or 6s integration period, resulting in a full radar sweep through all beams in 1 or 2 minutes. SuperDARN observations primarily consist of two types of backscatter, namely, ionospheric scatter and ground scatter. In the case of ground scatter, due to the high daytime vertical gradient in the refractive index, the rays bend toward the ground and are reflected from surface roughness and return to the radar following the same paths. Ionospheric scatter is due to the reflection of the transmitted signal from ionospheric plasma irregularities. However, in this study, we will only use the ground scatter observations. Specifically, we use the “inverse ground scatter count” during a particular period, determined as the drop in ground scatter echo counts during an event (i.e., maximum count – actual count) to estimate the ionospheric sluggishness observed by the HF radars (Chakraborty et al., 2018).

Figure 2 presents the location of the instruments used in this study. Radar fields-of-view of SuperDARN radars located in middle and high latitudes across the North American sectors are colored in red and blue, respectively. The fields-of-view indicated by the shading indicates the region of the ionosphere where SuperDARN is likely to be sensitive to solar flare driven fadeout-induced absorption spanning range gates 1-7. The green circles centered around the black dots represent the riometers used in this study. These filled circles denoting riometer station locations indicate the 100-km diameter region around each riometer station where absorption is detected.

3. Results

In this section, we characterize ionospheric sluggishness measured from riometer and SuperDARN observations, using the equations defined in Section 1 and describe a technique to estimate α_{eff} from the sluggishness measured by the riometer. Specifically, we present one classic example of ionospheric sluggishness in SuperDARN observations extracted using the peak time derivative and correlation methods proposed in Section 1. Next, we will statistically characterize $\bar{\delta}$ measured in the riometer observations and describe its dependence on χ , ϕ , LT, and I_{∞} . Then, we discuss the typical practice of using solar SXR as a reference to measure sluggishness and compare it with the measurement considering solar HXR as a reference. Finally, we describe a theoretical method to estimate α_{eff} from the sluggishness measured by the riometer ($\bar{\delta}$), validate it with the theoretical values, and get an insight into the D region chemistry. Note, unlike other two sluggishness, defined by equations (3) and (4), $\bar{\delta}$ can only be used to estimate α_{eff} , hence, we used $\bar{\delta}$ estimates from riometer observations to characterize the behavior of the sluggishness.

3.1 SuperDARN Event Study: 11 March 2015

As an example, consider an X2.1 solar x-ray flare that erupted on 11 March 2015, peaking at 16:22 UT. Fiori et al. (2018) used this event to demonstrate the potential of SuperDARN for monitoring the space weather impact due to solar X-ray flares due to the widespread observation of the event across Canada and the Northern United States.

Figure 3 presents a time series of inverse ground scatter count data from the SuperDARN Blackstone radar (black) in response to the sudden increase in solar SXR due to a solar flare (red) on 11 March 2015. The dashed red curve represents time delayed SXR data. The difference in timing of the peaks in the time derivatives, indicated by the red and black vertical dotted lines, represents the sluggishness associated with the peak time derivative method, which is $\bar{\delta}_s = 38$ s. The sluggishness estimated using correlation analysis is $\bar{\delta}_c = 50$ s. Both sluggishness values are significantly lower than the values obtained from the riometer measurements using peak time derivative and correlation method, $\bar{\delta}_s = 139$ s and $\bar{\delta}_c = 80$ s, respectively (refer Figure 1(b-c)). This significant difference in the sluggishness measured by the two instruments is most likely due to differences in their operating frequencies and the fact that riometers are passive receivers and operate in a vertical mode while the SuperDARN radars are active oblique sounders.

3.2 Correlation Analysis

To characterize the statistical behavior of $\bar{\delta}$ estimated from riometer observations, we choose 92 C, 63 M, and 18 X class solar flare events between 2006 to 2017. Note that, these solar flare events were selected from GOES XRS reports maintained by NOAA when the NRCAN riometers were online, to ensure the largest possible data set, and predominantly located on the dayside such that several riometers observed absorption enhancements in association with the enhanced solar X-ray flux. Finally, we choose events showing an absorption peak of at least 0.5 dB and at least 0.2 dB greater than the minimum absorption during the flare interval. Each solar flare event affects 4-5 riometers on average, and 640 individual riometer absorption events were collectively observed, in total.

Figure 4 presents a correlation analysis of the $\bar{\delta}$ observed by riometers with χ , ϕ , local time (LT), and I_{∞}^{max} (panels a-d), while panel (e) shows a generalized linear regression of $\bar{\delta}$ versus these four factors. A separate analysis is presented for C, M, and X class flares in the top, middle, and bottom rows, respectively. The correlation coefficients are listed inside each panel. This analysis shows the typical range of $\bar{\delta}$ is the 60s-1500s, which is in contrast with a reported range of δ^{VLF} , typically 5-10 minutes (Hayes et al., 2017; Palit et al., 2015). In the left-most column, it can be seen that $\bar{\delta}$ has a relatively higher positive correlation with χ for C and M class flares and shows almost no correlation for X-class flares. By contrast, the correlation of delta with latitude shows $\bar{\delta}$ shows almost no correlation for C-class flares, and correlation increases with flare class, as presented in the second left column. Besides, $\bar{\delta}$ does not show any linear dependence on local time as shown in the middle column, $\bar{\delta}$ does not have a linear dependence on LT for C, M, and X class flares. Sluggishness $\bar{\delta}$ shows negative correlations with I_{∞} , with the highest correlation coefficient for M-class flares as shown in the second right column. Note that for C-class flares shows no correlation with I_{∞} . Finally, the generalized linear regression of $\bar{\delta}$ versus the four factors, shown in the rightmost column. The models do a reasonably good job reproducing measured $\bar{\delta}$ (i.e., the correlation coefficient is high).

3.3 Hard X-ray Waveband as Reference

Ever since Appleton first developed the theory of ionospheric sluggishness most of the observational VLF studies have considered the peak of solar SRX irradiance as the reference time for estimating sluggishness (Ellison, 1953; Kvirivský, 1962; Palit et al., 2015), under the assumption that solar SRX irradiance is the best proxy for the photoionization. However, photoionization at different altitudes is regulated by solar irradiance wavebands, which peak at different times during a solar flare (Huang et al., 2014). Consequently, the reference time should vary with ionospheric heights, which creates ambiguity when estimating sluggishness from height integrated ionospheric response considering SXR data as the only reference.

Figure 5 presents one example of the issue described in the previous paragraph. Panels (a) and (b) present sluggishness estimated using conventional and peak time derivative methods from Ottawa riometer measurements during a solar flare event on 11 March 2015, considering SXR irradiance (in red) and HXR irradiance (in black) as a reference, respectively. Black dots represent observations from the Ottawa riometer. The estimated sluggishness using conventional and peak time derivative methods considering SXR irradiance as the reference is $\bar{\delta} = 46s$ and $\bar{\delta}_s = 139s$, respectively. In contrast, using HXR irradiance as reference the corresponding estimates for sluggishness are $\bar{\delta} = 91s$ and $\bar{\delta}_s = 151s$. There is thus a substantial difference in sluggishness estimation using HXR as a reference over SXR.

3.4 Theoretical Study: Effective Recombination Coefficient, α_{eff}

The focus of this section is to examine how chemical processes in the D region may play a role in regulating ionospheric sluggishness and estimate α_{eff} from the conventional sluggishness, $\bar{\delta}$, measured from riometer observations. There are a plethora of chemistry models exist that describe D region dynamics in terms of following constituents: electrons, positive ions, anions, and heavy positive ions or cluster ions (Glukhov et al., 1992; McRae & Thomson, 2004; Mitra, 1974; Mitra &

Jain, 1963; Žigman et al., 2007). Glukhov-Pasko-Inan (GPI) is a widely recognized model that describes chemistry in D region altitudes (Glukhov et al., 1992). In brief, the GPI model describes the ionosphere as a mixture of four constituents: electrons (n_e), negative ions (n^-), positive ions (n^+), and heavy positive cluster ions (n_x^+). Assuming charge neutrality, the effective recombination coefficient is

$$\alpha_{eff} = \left[\frac{\beta - \gamma\lambda}{n_e} + \alpha_d^c \frac{n_x^+}{n_e} + \alpha_d \right] = \alpha_{eff}^{n^-} + \alpha_{eff}^{n_x^+} + \alpha_{eff}^{n^+} \quad (6)$$

where: q , γ , β , α_d , α_d^c , and λ represent photoionization rate, electron detachment rate, electron attachment rate, electron-ion dissociative coefficient, electron-cluster ion dissociative coefficient, and negative ion to electron ratio, respectively. Note that the GPI model uses relatively constant values of α_d and α_d^c for D region heights, however, γ and β are functions of electron temperature (T_e) (Glukhov et al., 1992; Lehtinen & Inan, 2007). The effective recombination coefficient, α_{eff} , depends on negative ion chemistry (first term, $\alpha_{eff}^{n^-}$), positive cluster ion chemistry (second term, $\alpha_{eff}^{n_x^+}$), and dissociative recombination rates (third term, $\alpha_{eff}^{n^+}$), with typical ranges of values $10^{-11} - 10^{-12} \text{ m}^3\text{s}^{-1}$, $10^{-11} - 10^{-12} \text{ m}^3\text{s}^{-1}$, and $3 \times 10^{-13} - 10^{-13} \text{ m}^3\text{s}^{-1}$, respectively (Ananthakrishnan et al., 1973; Schunk & Nagy, 2009). Alternatively, a study by Žigman (2007) showed that α_{eff} can be estimated from measured δ , peak electron density, and irradiance flux as:

$$\alpha_{eff} = \frac{3}{8\delta \left(n_e^{max} - \frac{I_{\infty}^{max} \delta g m_{avg}}{\rho e k T} \cos \chi \right)} \quad (7)$$

where: e is the base of the natural logarithm, k is the Boltzmann constant, g is the gravitational acceleration, $m_{avg} = 4.8 \times 10^{-26} \text{ kg}$ is the mean molecular mass (Mitra, 1992), $\rho = 34 \text{ eV}$ is the average energy required to produce one electron-ion pair (Whitten et al., 1965), and $T \sim 210 \text{ K}$ is the averaged electron temperature of the D region (Schmitter, 2011; Sharma et al., 2004).

We used equation (7) with simplified D region assumptions¹ to estimate α_{eff} from sluggishness measured from riometer observations using the conventional method, $\bar{\delta}$. Figure 6 presents the results of using this approach. Specifically, panel (a) shows estimated peak electron density at 74.1km heights and for $\chi \sim 60^\circ - 80^\circ$ following Žigman et al. (2007) (in red), $\bar{\delta}$ from riometer measurement for $\chi \sim 60^\circ - 80^\circ$ (in blue dots), and fitted $\bar{\delta}$ (in the blue curve). Panel (b) shows variations in estimated α_{eff} from equation (7), with peak solar flux intensity. Regions shaded in blue, green, and red show typical ranges of $\alpha_{eff}^{n^-}$, $\alpha_{eff}^{n_x^+}$, and $\alpha_{eff}^{n^+}$, respectively (Glukhov et al., 1992). Note for C class flares α_{eff} remains almost constant and within the negative and cluster ion chemistry region shaded blue. However, with increasing peak solar irradiance α_{eff} decreases, and the value drops below $10^{-14} \text{ m}^3\text{s}^{-1}$. The slope of the line is $m =$

¹ Assumptions: i. D region is one thin layer; ii. all sluggishness in riometer measurements $\bar{\delta}$ coming from the D region, this implies $\bar{\delta} \approx \delta$ and $\bar{\alpha}_{eff} \approx \alpha_{eff}$; iii. n_e^{max} is taken from Žigman (2007) considering D region is one thin layer concentrated around $h \sim 74.1 \text{ km}$ and $\chi > 50^\circ$.

– $7.72 \times 10^{-2} \text{ m}^3\text{s}^{-1}/10 \text{ Wm}^{-2}$. One explanation for this drop-in D region α_{eff} could be an increase in D region electron density and a decrease in electron photo-detachment rate under the influence of the increased solar irradiance.

4. Discussion

In this study, we have defined two new methods to estimate ionospheric sluggishness $\bar{\delta}_s$ and $\bar{\delta}_c$ using maximum slope and correlation analysis. In addition, we compared estimates of ionospheric sluggishness using both passive and active high frequency (HF, 3–30 MHz) instruments, namely riometers and SuperDARN HF radars, respectively. Furthermore, we did a comprehensive characterization of $\bar{\delta}$ using riometers following 92 C, 63 M, and 18 X-class flares that occurred between 2006 and 2017 (Figure 4). We have also presented a comparison between the sluggishness estimated, considering SXR and HXR (Figure 5). Finally, we used theoretical arguments to estimate α_{eff} from measured $\bar{\delta}$ and gain some insights into the D region chemistry (Figure 6). In this section, we summarize the findings and discuss how they inform our understanding of the physical processes that control ionospheric sluggishness.

As noted previously, sluggishness is an inertial property of the ionosphere (Basak & Chakrabarti, 2013; Ellison, 1953). Early studies claimed that sluggishness is related to recombination processes and inversely proportional to the product of electron density and α_{eff} , where α_{eff} is relatively constant for a particular latitude, local time and height. If this were the case, sluggishness would only be a function of electron density (Palit et al., 2015). However, in this study, we found the measured sluggishness varies significantly with the measuring techniques (see Figures 1 and 2), and we also found the estimation of sluggishness using the peak time derivative (equation 3) is greater than that using the conventional definition (equation 2). The probable reason might be larger electron density during the peak of solar flare event than before the peak. This implies that ionospheric sluggishness is indeed inversely proportional to electron density but does not confirm that α_{eff} is a constant. Furthermore, this explanation does not fit the reasoning for the smaller values of sluggishness from SuperDARN HF radar observations using the modified definition (refer Figure 3). The most likely explanation is the difference in the ionospheric sounding techniques between the instruments. For example, SuperDARN rays traverse the D region four times and at a lower operating frequency, hence, they are more sensitive to the D region perturbations. Taking all these factors together we can conclude that the choice of ionospheric sounding technique impacts the sluggishness measurement. What matters then, are the relative differences in sluggishness measured by a single instrument under different conditions.

The choice of solar irradiance also impacts the sluggishness estimation, as presented in Figure 5. Historically, SXR has been used as reference data to estimate sluggishness (e.g., Palit et al., 2015), the assumption being that SXR characterizes the intensity of ionizing radiation at D region altitudes. However, HXR also produces a significant amount of ionization at the lower D region heights, and photoionization at different heights is regulated by different solar irradiance wavebands that peak at different times during solar flares (Huang et al., 2014). Moreover, because riometer observations provide a height integrated measurement of HF absorption, it is difficult to know the exact relationship of sluggishness estimates to ionospheric parameters without the help of modeling efforts. Hence, the question arises, which reference waveband should we use to extract sluggishness from the riometer measurements? We

suggest referring to the ionizing solar radiation wavebands that have an optical depth associated with the altitude that is equal to the altitude of maximum HF absorption.

From the correlation analysis (Figure 4), we found that $\bar{\delta}$ is positively associated with increasing solar zenith angle and decreasing solar SXR intensity, which is consistent with previous VLF studies (Basak & Chakrabarti, 2013; Palit et al., 2015). These results are consistent with the physics described by Appleton (1953), namely that an increase in solar zenith angle produces a decrease in photoionization and electron density, which leads to an increase in ionospheric sluggishness. Naively, one might expect sluggishness to also decrease with latitude for similar reasons; however, panels b-1~3 show a high correlation of $\bar{\delta}$ with latitude, but only for M and X class flares. One possible explanation for this mixed latitude dependence is variability in α_{eff} which is known to have a strong dependence on anionic chemistry at higher latitudes (Amemiya & Nakamura, 1996; Mitra, 1974). Further detailed analysis and modeling of sluggishness across latitudes and local time may provide further insights into the variability of D region chemistry. Future work will also examine the statistical behavior of $\bar{\delta}_c$ and $\bar{\delta}_s$ measured from riometer and SuperDARN observations.

Another focus of this study has been to estimate α_{eff} from $\bar{\delta}$ measured using riometer measurements. Equation (6) describes the effective recombination coefficient in terms of negative ion formation and destruction (first term α_{eff}^{n-}), dissociative electron-cluster ion recombination (second term $\alpha_{eff}^{n_x^+}$), and dissociative electron-ion recombination (third term $\alpha_{eff}^{n^+}$) (Glukhov et al., 1992; Schunk & Nagy, 2009; Žigman et al., 2007). We have shown the effective ionospheric recombination coefficient (α_{eff}) varies by several orders of magnitude (typically between $10^{-11} - 10^{-14} \text{ m}^3\text{s}^{-1}$) with peak solar SXR irradiance (Figure 6). The range of values for α_{eff} is consistent with those found in previous literature (García-Rigo et al., 2007; Gledhill, 1986; Schunk & Nagy, 2009). We conclude that reductions in estimated α_{eff} are mainly due to drops in the negative and positive cluster ion effective recombination coefficients denoted by α_{eff}^{n-} and $\alpha_{eff}^{n_x^+}$, respectively. Specifically, decreases in α_{eff} are caused by enhancements in electron density (n_e) due to photoionization and to enhancements in electron detachment rate (γ) due to the sudden rise of molecular vibrational and rotational energy under the influence of energetic EM radiation (Verronen et al., 2006). Taken all together, we conclude that intense solar flares alter the negative and positive ion chemistry at the D-region altitudes. Recent studies have suggested that an increase in flare time D-region electron temperature that changes the electron-ion dissociative coefficient (α_d) can lead to an overall drop in the effective recombination coefficient (see Figure 5 in Nina et al., 2012; Bajcetic et al., 2015). More detailed data analysis and modeling efforts are required to fully understand D-region negative ion and positive cluster ion chemistry during solar flares and how it is affected by changes in D-region electron temperature.

5. Conclusion

In this study, we have compared estimates of ionospheric sluggishness obtained from riometer and SuperDARN HF radar observations using three different methodologies. A correlation analysis was conducted on the sluggishness estimated from riometer observations using a conventional method. We performed a simulation study to estimate the effective recombination coefficient (α_{eff}) and to examine its

variations with peak solar soft X-ray flux. We found that the choice of ionospheric sounding techniques and reference solar irradiance wavebands affects the estimation of sluggishness. We also found that ionospheric sluggishness is anti-correlated with solar EUV radiation intensity, as expected. We showed that the effective recombination coefficient (α_{eff}) varies by several orders of magnitude, typically between $10^{-11} - 10^{-14} \text{ m}^3\text{s}^{-1}$, with the flare time peak solar soft X-ray irradiance. The results suggest an increase in electron density and negative ion chemistry under the influence of EUV and X-ray flux is the major determinant of sluggishness. Future work will examine how sluggishness depends on latitudinal factors and complex-ion (negative and positive cluster ion) chemistry and geomagnetic activity.

Acknowledgments

SC thanks to the National Science Foundation for support under grant AGS-1341918. KAZ acknowledges support from the Chief of Naval Research (CNR) under the NRL 6.1 Base Program. We wish to acknowledge the use of the NOAA/GOES X-ray data (from <https://satdat.ngdc.noaa.gov/sem/goes/data/>) for flare confirmation and analysis. We thank NRCAN for providing the riometer data and the University of Calgary for providing riometer data directly via <http://data.phys.ucalgary.ca/>. We also thank all participants in the worldwide SuperDARN collaboration for the distribution of SuperDARN data via <http://vt.superdarn.org/tiki-index.php?page=Data+Access>. The majority of analysis and visualization was completed with the help of free, open-source software tools such as matplotlib (Hunter, 2007), IPython (Perez & Granger, 2007), pandas (McKinney, 2010), Spacepy (S. K. Morley et al., 2011), PyForecastTools (S. Morley & Burrell, 2020), and others (e.g., Millman & Aivazis, 2011).

References

- Amemiya, H., & Nakamura, Y. (1996). Measurement of Negative Ions in the Lower Ionosphere (D-Layer) in the Polar Region. *Journal of Geomagnetism and Geoelectricity*, 48(4), 391–401. <https://doi.org/10.5636/jgg.48.391>
- Ananthakrishnan, S., Abdu, M. A., & Piazza, L. R. (1973). D-region recombination coefficients and the short wavelength X-ray flux during a solar flare. *Planetary and Space Science*, 21(3), 367–375. [https://doi.org/10.1016/0032-0633\(73\)90035-4](https://doi.org/10.1016/0032-0633(73)90035-4)
- Appleton, E. V. (1953). A note on the “sluggishness” of the ionosphere. *Journal of Atmospheric and Terrestrial Physics*, 3(5), 282–284. [https://doi.org/10.1016/0021-9169\(53\)90129-9](https://doi.org/10.1016/0021-9169(53)90129-9)
- Bajcetic, J., Nina, A., Cadez, V. M., & Todorovic, B. (2015). Ionospheric D-region temperature relaxation and its influences on radio signal propagation after solar X-flares occurrence. *Thermal Science*, 19, 84. <https://doi.org/10.2298/TSCI141223084B>
- Basak, T., & Chakrabarti, S. K. (2013). Effective recombination coefficient and solar zenith angle effects on low-latitude D-region ionosphere evaluated from VLF signal amplitude and its time delay during X-ray solar flares. *Astrophysics and Space Science*, 348(2), 315–326. <https://doi.org/10.1007/s10509-013-1597-9>
- Bland, E. C., Heino, E., Kosch, M. J., & Partamies, N. (2018). SuperDARN radar-derived HF radio attenuation during the September 2017 solar proton events. *Space Weather*. <https://doi.org/10.1029/2018SW001916>
- Browne, S., Hargreaves, J. K., & Honary, B. (1995). An imaging riometer for ionospheric studies. *Electronics and Communication Engineering Journal*, 7(5), 209–217. <https://doi.org/10.1049/ecej:19950505>
- Chakraborty, S., Baker, J. B. H., Ruohoniemi, J. M., Kunduri, B., Nishitani, N., & Shepherd, S. G. (2019). A Study of SuperDARN Response to Co-occurring Space Weather Phenomena. *Space Weather*, 17(9), 1351–1363. <https://doi.org/10.1029/2019SW002179>
- Chakraborty, S., Ruohoniemi, J. M., Baker, J. B. H., & Nishitani, N. (2018). Characterization of Short-Wave Fadeout Seen in Daytime SuperDARN Ground Scatter Observations. *Radio Science*, 53(4), 472–484. <https://doi.org/10.1002/2017RS006488>
- Chisham, G., Lester, M., Milan, S. E., Freeman, M. P., Bristow, W. A., Grocott, A., MacWilliams, K. A., Ruohoniemi, J. M., Yeoman, T. K., Dyson, P., Greenwald, R. A., Kikuchi, T., Pinnock, M., Rash, J., Sato, N., Sofko, G., Villain, J.-P., & Walker, A. D. M. (2007). A Decade of the Super Dual Auroral Radar Network (SuperDARN): Scientific achievements, new techniques and future directions. *Surveys in Geophysics*, 28, 33–109. <https://doi.org/doi:10.1007/s10712-007-9017-8>
- Dellinger, J. H. (1937). Sudden ionospheric disturbances. *Journal of Geophysical Research*, 42(1), 49. <https://doi.org/10.1029/te042i001p00049>

- Ellison, M. A. (1953). The H α radiation from solar flares in relation to sudden enhancements of atmospherics on frequencies near 27 Kc/s. *Journal of Atmospheric and Terrestrial Physics*, 4(4–5), 226–239. [https://doi.org/10.1016/0021-9169\(53\)90057-9](https://doi.org/10.1016/0021-9169(53)90057-9)
- Fiori, R. A. D., & Danskin, D. W. (2016). Examination of the relationship between riometer-derived absorption and the integral proton flux in the context of modeling polar cap absorption. *Space Weather*, 14(11), 1032–1052. <https://doi.org/10.1002/2016SW001461>
- Fiori, R. A. D., Koustov, A. V, Chakraborty, S., Ruohoniemi, J. M., Danskin, D. W., Boteler, D. H., & Shepherd, S. G. (2018). Examining the potential of the Super Dual Auroral Radar Network for monitoring the space weather impact of solar X-ray flares. *Space Weather*, 0(ja).
- García-Rigo, A., Hernández-Pajares, M., Juan, J. M., & Sanz, J. (2007). Solar flare detection system based on global positioning system data: First results. *Advances in Space Research*, 39(5), 889–895. <https://doi.org/10.1016/j.asr.2006.09.031>
- Gledhill, J. A. (1986). The effective recombination coefficient of electrons in the ionosphere between 50 and 150 km. *Radio Science*, 21(3), 399–408. <https://doi.org/10.1029/RS021i003p00399>
- Glukhov, V. S., Pasko, V. P., & Inan, U. S. (1992). Relaxation of transient lower ionospheric disturbances caused by lightning-whistler-induced electron precipitation bursts. *Journal of Geophysical Research*, 97(A11), 16971. <https://doi.org/10.1029/92ja01596>
- Greenwald, R. A., Baker, K. B., Hutchins, R. A., & Hanuise, C. (1985). An HF Phased-Array Radar for Studying small-scale Structure in the High-Latitude Ionosphere. *Radio Science*, 20(1), 63–79. <https://doi.org/10.1029/RS020i001p00063>
- Hayes, L. A., Gallagher, P. T., McCauley, J., Dennis, B. R., Ireland, J., & Inglis, A. (2017). Pulsations in the Earth’s Lower Ionosphere Synchronized With Solar Flare Emission. *Journal of Geophysical Research: Space Physics*, 122(10), 9841–9847. <https://doi.org/10.1002/2017JA024647>
- Huang, Y., Richmond, A. D., Deng, Y., Chamberlin, P. C., Qian, L., Solomon, S. C., Roble, R. G., & Xiao, Z. (2014). Wavelength dependence of solar irradiance enhancement during X-class flares and its influence on the upper atmosphere. *Journal of Atmospheric and Solar-Terrestrial Physics*, 115–116, 87–94. <https://doi.org/10.1016/j.jastp.2013.10.011>
- Hunter, J. D. (2007). Matplotlib: A 2D graphics environment. *Computing in Science and Engineering*, 9(3), 99–104. <https://doi.org/10.1109/MCSE.2007.55>
- Kvřivský, L. (1962). Flare maximum and the “sluggishness” of the ionospheric D-region. *Bulletin of the Astronomical Institutes of Czechoslovakia*, 13, 59.
- Lam, H.-L. (2011). From Early Exploration to Space Weather Forecasts: Canada’s Geomagnetic Odyssey. *Space Weather*, 9(5), <https://doi.org/10.1029/2011sw000664>
- Lehtinen, N. G., & Inan, U. S. (2007). Possible persistent ionization caused by giant blue jets. *Geophysical Research Letters*, 34(8).

- 506 <https://doi.org/10.1029/2006GL029051>
- 507 Machol, J. (2016). *GOES X-ray Sensor (XRS) Measurements Important notes for users*.
- 508 McKinney, W. (2010). Data Structures for Statistical Computing in Python. In S. van
- 509 der Walt & J. Millman (Eds.), *Proceedings of the 9th Python in Science*
- 510 *Conference* (pp. 51–56).
- 511 McRae, W. M., & Thomson, N. R. (2004). Solar flare induced ionospheric D-region
- 512 enhancements from VLF phase and amplitude observations. *Journal of*
- 513 *Atmospheric and Solar-Terrestrial Physics*, 66(1), 77–87.
- 514 <https://doi.org/10.1016/j.jastp.2003.09.009>
- 515 Millman, K. J., & Aivazis, M. (2011). Python for scientists and engineers. In
- 516 *Computing in Science and Engineering* (Vol. 13, Issue 2, pp. 9–12).
- 517 <https://doi.org/10.1109/MCSE.2011.36>
- 518 Mitra, A. P. (1974). *Ionospheric Effects of Solar Flare* (Vol. 46). Astrophysics and
- 519 Space Science Library. <https://doi.org/10.1007/978-94-010-2231-6>
- 520 Mitra, A. P., & Jain, V. C. (1963). Interpretation of the observed zenith-angle
- 521 dependence of ionospheric absorption. *Journal of Geophysical Research*, 68(9),
- 522 2367–2373. <https://doi.org/10.1029/jz068i009p02367>
- 523 Morley, S. K., Koller, J., Welling, D. ~T., Larsen, B. ~A., Henderson, M. ~G., & Niehof,
- 524 J. ~T. (2011). Spacepy - A Python-based library of tools for the space sciences.
- 525 *Proceedings of the 9th Python in Science Conference (SciPy 2010)*.
- 526 Morley, S., & Burrell, A. (2020). *drsteve/PyForecastTools: Version 1.1.1*.
- 527 <https://doi.org/10.5281/ZENODO.3764117>
- 528 Nina, A., Čadež, V., Šulić, D., Srećković, V., & Žigman, V. (2012). Effective electron
- 529 recombination coefficient in ionospheric D-region during the relaxation regime
- 530 after solar flare from February 18, 2011. *Nuclear Instruments and Methods in*
- 531 *Physics Research, Section B: Beam Interactions with Materials and Atoms*, 279,
- 532 106–109. <https://doi.org/10.1016/j.nimb.2011.10.026>
- 533 Nishitani, N., Ruohoniemi, J. M., Lester, M., Baker, J. B. H., Koustov, A. V., Shepherd,
- 534 S. G., Chisham, G., Hori, T., Thomas, E. G., Makarevich, R. A., Marchaudon, A.,
- 535 Ponomarenko, P., Wild, J. A., Milan, S. E., Bristow, W. A., Devlin, J., Miller, E.,
- 536 Greenwald, R. A., Ogawa, T., & Kikuchi, T. (2019). Review of the
- 537 accomplishments of mid-latitude Super Dual Auroral Radar Network
- 538 (SuperDARN) HF radars. *Progress in Earth and Planetary Science*, 6(1), 27.
- 539 <https://doi.org/10.1186/s40645-019-0270-5>
- 540 Palit, S., Basak, T., Pal, S., & Chakrabarti, S. K. (2015). Theoretical study of lower
- 541 ionospheric response to solar flares: sluggishness of D-region and peak time delay.
- 542 *Astrophysics and Space Science*, 356(1), 19–28. [https://doi.org/10.1007/s10509-](https://doi.org/10.1007/s10509-014-2190-6)
- 543 [014-2190-6](https://doi.org/10.1007/s10509-014-2190-6)
- 544 Pequignot, D., Petitjean, P., & Boisson, C. (1991). Total and effective radiative
- 545 recombination coefficients. *Aap*, 251, 680–688.
- 546 Perez, F., & Granger, B. E. (2007). IPython: A System for Interactive Scientific
- 547 Computing. *Computing in Science & Engineering*, 9(3), 21–29.
- 548 <https://doi.org/10.1109/MCSE.2007.53>

- 549 Reid, G. C. (1970). {P}roduction and loss of electrons in the quiet daytime {D} region
550 of the ionosphere. *Journal of Geophysical Research (1896-1977)*, 75(13), 2551–
551 2562. <https://doi.org/10.1029/JA075i013p02551>
- 552 Rostoker, G., Samson, J. C., Creutzberg, F., Hughes, T. J., McDiarmid, D. R.,
553 McNamara, A. G., Jones, A. V., Wallis, D. D., & Cogger, L. L. (1995). Canopus
554 - A ground-based instrument array for remote sensing the high latitude ionosphere
555 during the ISTEP/GGS program. *Space Science Reviews*, 71(1–4), 743–760.
556 <https://doi.org/10.1007/BF00751349>
- 557 Schmitter, E. D. (2011). Remote sensing planetary waves in the midlatitude mesosphere
558 using low frequency transmitter signals. *Annales Geophysicae*, 29(7), 1287–1293.
559 <https://doi.org/10.5194/angeo-29-1287-2011>
- 560 Schunk, R., & Nagy, A. (2009). *Ionospheres: Physics, Plasma Physics, and Chemistry*
561 (2nd ed.). Cambridge University Press.
562 <https://doi.org/10.1017/CBO9780511635342>
- 563 Sharma, D. K., Rai, J., Israil, M., Subrahmanyam, P., Chopra, P., & Garg, S. C. (2004).
564 Enhancement in electron and ion temperatures due to solar flares as measured by
565 SROSS-C2 satellite. *Annales Geophysicae*, 22(6), 2047–2052.
566 <https://doi.org/10.5194/angeo-22-2047-2004>
- 567 Verronen, P. T., Ulich, T., Turunen, E., & Rodger, C. J. (2006). Sunset transition of
568 negative charge in the D-region ionosphere during high-ionization conditions.
569 *Annales Geophysicae*, 24(1), 187–202. [https://doi.org/10.5194/angeo-24-187-](https://doi.org/10.5194/angeo-24-187-2006)
570 2006
- 571 Whitten, R. C., Poppoff, I. G., Edmonds, R. S., & Berning, W. W. (1965). Effective
572 recombination coefficients in the lower ionosphere. *Journal of Geophysical*
573 *Research*, 70(7), 1737–1742. <https://doi.org/10.1029/jz070i007p01737>
- 574 Žigman, V., Grubor, D., & Šulić, D. (2007). D-region electron density evaluated from
575 VLF amplitude time delay during X-ray solar flares. *Journal of Atmospheric and*
576 *Solar-Terrestrial Physics*, 69(7), 775–792.
577 <https://doi.org/10.1016/j.jastp.2007.01.012>
- 578

Figures & Captions

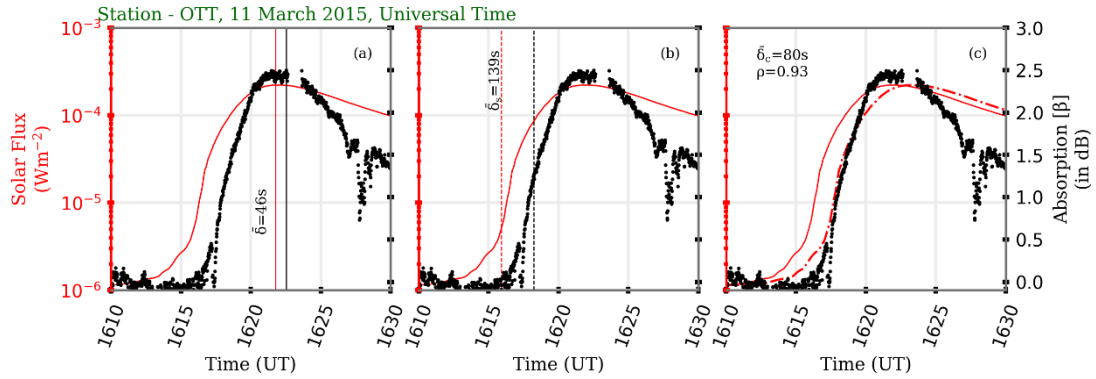


Figure 1. Ionospheric sluggishness in Ottawa (OTT) riometer measurement during a solar flare event on 11 March 2015, estimated using (a) conventional, (b) peak time derivative, and (c) correlation methods. Red and black colors represent SXR irradiance from GOES and CNA observations from the riometer, respectively. The solid and dashed vertical lines in panels (a) and (b) represent peaks and peak time derivative in both datasets, respectively. The dashed red curve in panel (c) represents time delayed GOES SXR irradiance data. Sluggishness values estimated using the three different methods are provided inside each panel.

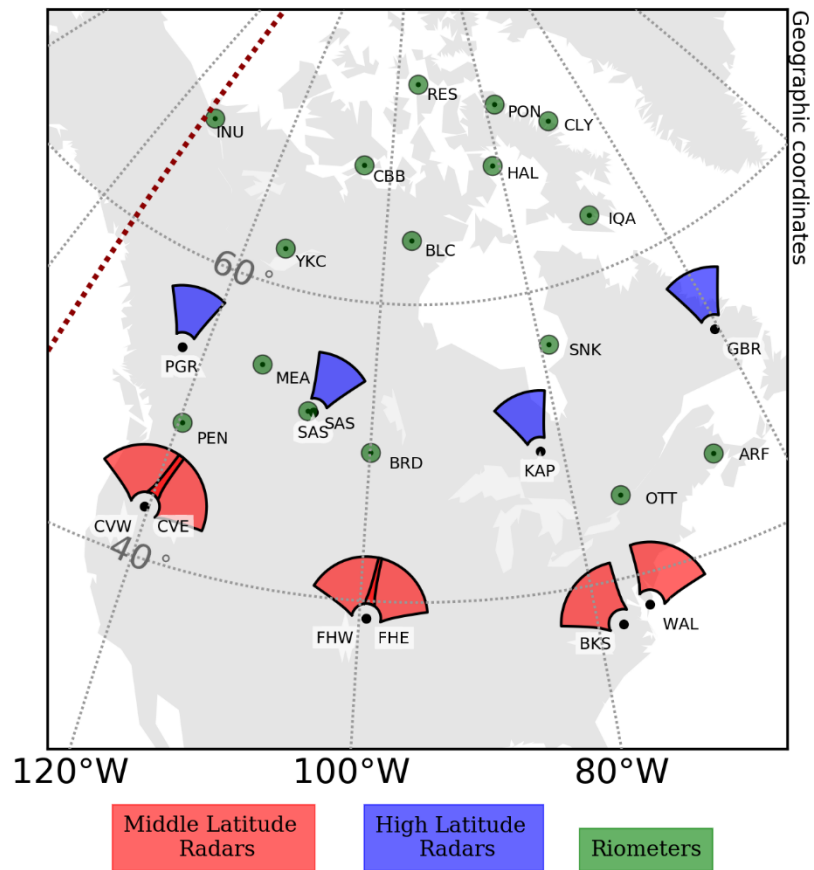


Figure 2. Location of the various instruments used in the study. The red line at -135.3° longitude indicates the longitudinal location of the GOES 15 satellite. Colors represent the fields-of-view of the middle (red) and high (blue) latitude SuperDARN radars and riometers (green).

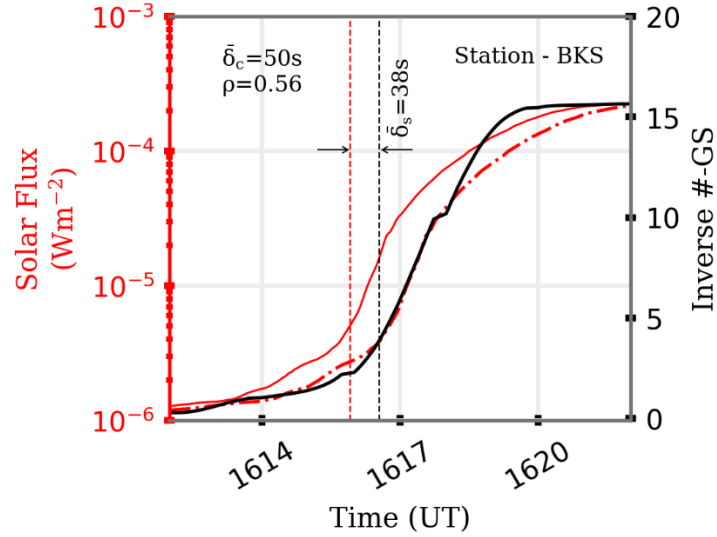


Figure 3. Ionospheric sluggishness in SuperDARN Blackstone radar ground scatter measurements estimated using peak time derivative and correlation methods during a solar flare event on 11 March 2015. Red and black colors represent SXR irradiance from GOES, and inverse ground scatter echoes from Blackstone SuperDARN radar, respectively. The solid and dashed red curves represent actual and time-delayed SXR irradiance, respectively. The dashed vertical lines represent peak time derivatives in both the datasets. Sluggishness values estimated using peak time derivative, correlation methods, and correlation coefficient are provided in the panel.

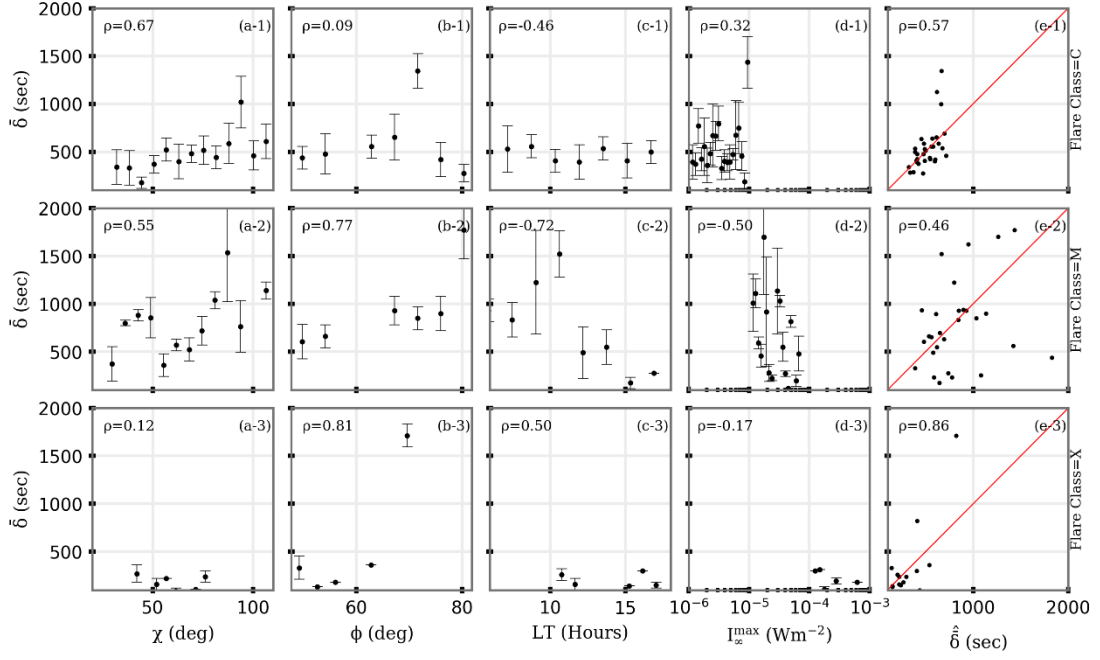


Figure 4. Correlation analysis between sluggishness estimated using equation (2) ($\bar{\delta}$) with (a-1~3) solar zenith angle (χ), (b-1~3) latitude (ϕ), (c-1~3) local time (LT), (d-1~3) peak flux (I_{∞}), respectively, and (e-1~3) generalized linear regression analysis of $\bar{\delta}$ and the four factors under consideration. C, M, and X class flare analyses are shown in the top, middle, and bottom row, respectively. Associated correlation coefficients are provided inside each panel.

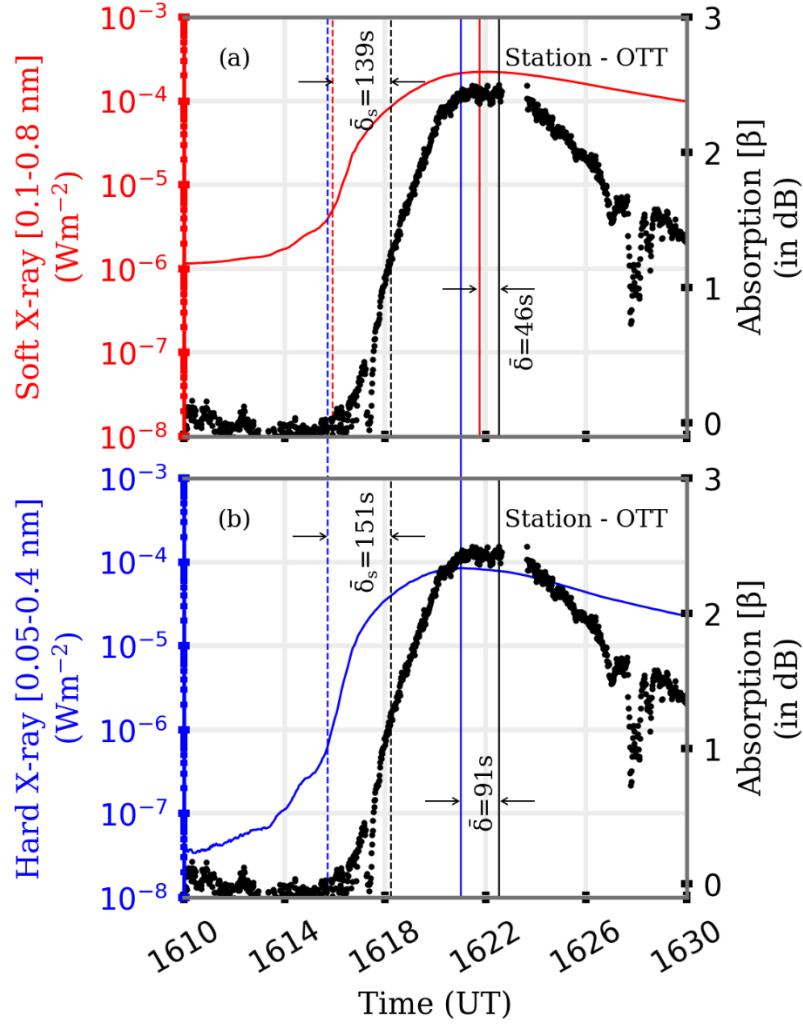


Figure 5. Sluggishness in Ottawa riometer measurement during a solar flare event on 11 March 2015, considering (a) SXR irradiance and (b) HXR irradiance observations as reference. Red, blue, and black colors represent SXR, HXR irradiance from GOES, and CNA observations from the riometer, respectively. The solid (dashed) red and black lines represent the peak times (peak time derivatives) in GOES SRX irradiance and riometer cosmic noise absorption, respectively. Sluggishness estimated using conventional and peak time derivative methods are mentioned in panels.

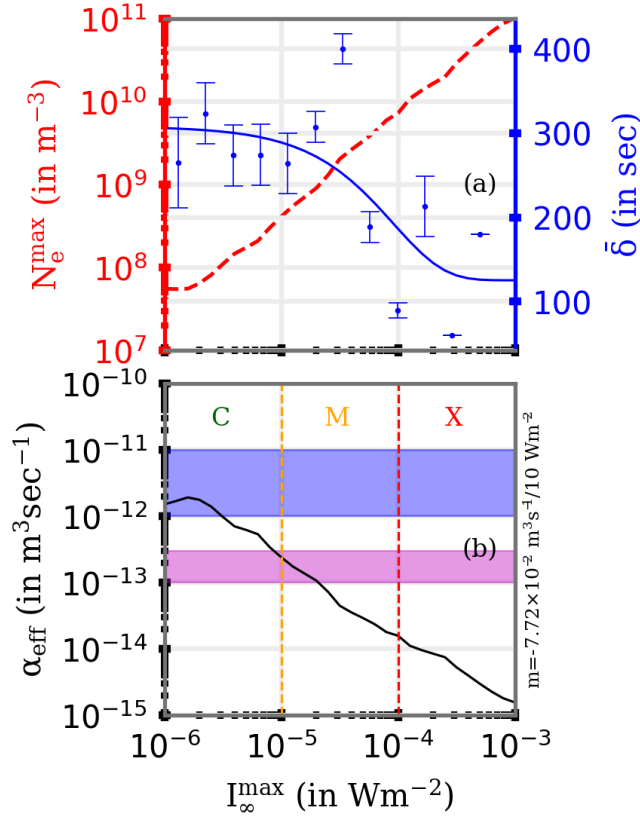


Figure 6. Model-data comparison of variations in (a) peak electron density at D region heights from Zigman et al. (2007) (in red) and $\bar{\delta}$ from riometer measurement for $\chi > 50^\circ$ (in blue dots), and (b) $\bar{\alpha}_{\text{eff}}$ from equation (13), with peak solar flux intensity. Blue smoothed line in panel (a) is the averaged $\bar{\delta}$. Vertical orange and red lines in panel (b) represent the separation between C, M, and X class flares. The slope of the black curve (m) in panel (b) is provided along the right vertical axis of the panel.